Supporting Information

Soft robots for cluttered environments based on origami anisotropic stiffness structure (OASS) inspired by desert iguana

Renjie Zhu, Dongliang Fan, Wenyu Wu, Chongshan He, Guojie Xu, Jian S. Dai*, and Hongqiang Wang*

*Corresponding author. Email: daijs@sustech.edu.cn; wanghq6@sustech.edu.cn

This PDF file includes:

Supplementary Text

Figures S1 to S14

Table S1

Movies S1 to S13

Other Supplementary Materials for this manuscript include the following:

Movies S1 to S13

Methods and Experiments

Fabrication

The manufacturing process of OASS molecules and actuators is shown in Figure S11. First, we engraved the 2D pattern on a paper using a CO_2 laser machine (HDZ-UVC3030, Han's Laser) by a low-power setting (4 W) and cut through the paper following the contour profile by a high-power pass (12 W; Figure S11A and S11B). Along these cuts, we folded the paper into molecules (Figure S11C and Movie S13). We used instant cyanoacrylate gel (Ergo 5210, Kisling) to attach triangle openings on both sides (Figure S11C). Similarly, OASS molecule tubes of different lengths can be created. For example, to make a 2×5 OASS actuator, we made two five-bulge molecule tubes and five two-bulge molecule tubes (Figure S11D). The five-bulge molecule tubes were bonded parallel by glue and then immersed into a mold filled with the silicone precursor (Ecoflex 00-30) for 4 hours until the silicone rubber was cured (Figure S11E and S11F). Next, five two-bulge tubes were glued upon the two-molecule-tube assembly by silicone adhesive (Sil-Poxy, Smooth-On; Figure S11G). Finally, all exposed surfaces of OASS actuator were covered with a layer of silicone rubber (Figure S11H). By combining these tubes in various topologies, actuators and robots with vast functions and shapes can be generated.

Robot assembly

In this work, we presented two crawling robots of different sizes. The small one is a 3×4 OASS actuator in which θ, l, and t are 60°, 19 mm, and 0.25 mm, respectively. An elastic membrane (Parafilm, Sigma-Aldrich) is wrapped on the outer layer to seal the body and increase the elasticity. The crawler is actuated using a vacuum pump (VP100, DaeirTuo) and 2/2 way pneumatic solenoid valves (TG22-08, STNC). On the other hand, the big crawling robot consists of 6×8 bulges, which θ is 60°, l is 30 mm, and t is 2.45 mm. Its skeleton is paper, and on the surfaces, silicone rubber (Ecoflex 00-30) is covered, outside of which is a plastic bag for sealing. Directional frictional metal sheets were attached at the bottom as feet (Figure S12) to propel the robot to move forwards during the operation of the actuator.

The robotic hand consists of five OASS fingers and a 3D-printed rigid palm (Figure 5A). The fingers have two bulges in width but different lengths - five, six, seven, six, and four bulges for the thumb, index, middle, ring, and little fingers, respectively. In these fingers, θ is 75°, l is 11 mm, and t is 0.45 mm.

We drove four DC motors (Motor 1-3: GM20-180; Motor 4: GM25-370, ChiHai Motor) to bend the fingers through cords (Figure 5A). All the fingers can be bent independently except that the ring finger and the little finger share the same motor (Motor 4; Figure S13). The thumb and the index fingers together are driven by a linear stepper (L12-30-100-6-I, Actuonix lnc.) to move translationally concerning the middle finger for clipping operation.

As shown in Figure S14, the control system comprises both on-board and off-board units, which communicate using Bluetooth 4.0 communication protocol via a wireless serial transceiver module (model TI CC2540, BLE-Link, DFRobot). The on-board system is fixed in the palm, which includes a micro-controller (model ATMega328, Arduino UNO) powered by a micro 3.7 V lithium battery (FIT0120, DFRobot) and four motors and a linear stepper powered by a 12 V power supply (UTP3313TFL-II, UNI-T). The off-board system is a remote controller (BLE Wireless Gamepad, DFRobot).

The snake-shaped robot is composed of a 2×6 and a 2×8 OASS actuator (θ, l, and t are 60°, 19 mm, and 0.45 mm, respectively) connected in series, and they are covered in a TPU seal bag. The robot is actuated using a vacuum pump via two 2/2 way pneumatic solenoid valves switching on and off alternately every 500 ms.
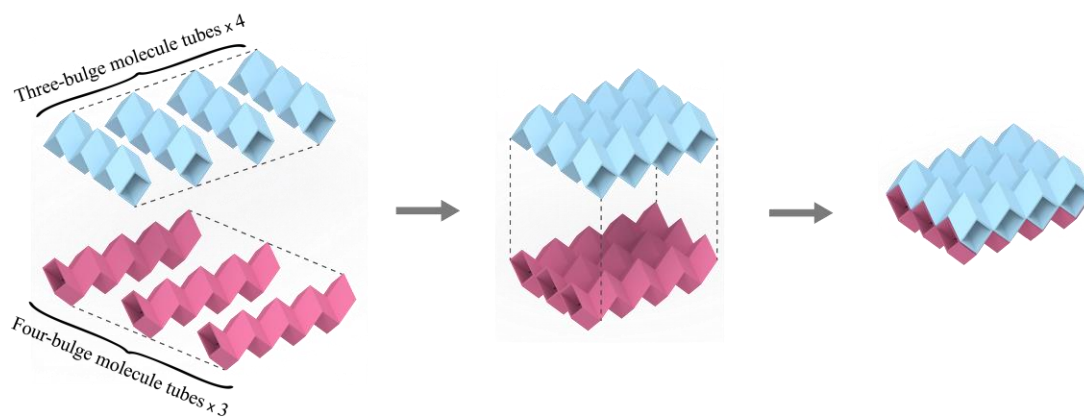
Simulation methods

To determine the compression and bending stiffness of the OASS actuator in different directions, we simulated uniaxial compression and bending tests using commercial software ABAQUS 2019. For convenience, the simulation model employs an isotropic, linear elastic material with an equivalent Young's Modulus (230 MPa) achieved from trial tests. For the compression test, the bottom points of bulges are entirely fixed, and the top points of each bulge are pressed down by a rigid body with 5 mm displacement. For the bending test, one end of the OASS actuator is completely fixed, and the other end is pressed down until the deflection reached 5 mm. Quadratic order cubic C3D20 elements with normal integration are employed in the model to obtain accurate results, and the mesh size is 1 mm. In this way, OASS actuators with various thicknesses, angles, and numbers of bulges are simulated.

Experimental methods of reliability test

We conducted a series of tests to verify the influence of the silicone layer covering the paper skeleton. We compressed the samples [3×4 OASS actuators under various values of θ (45°, 60°, and 70°)] vertically at a constant rate of 10 mm/min in two directions with a load cell (DS2-

500N-S, ZhiQu Co., Ltd.) installed on the moving stage of a universal tensile test machine (ZQ-990LA, ZhiQu; Figure S7). The structure for each parameter has five samples made of different materials, e.g., PLA (eSUN), F-PLA(eSUN), TPE(eSUN), PP, and SP. In the bending stiffness test (Figure S8), the samples [2×5 OASS actuators under various values of θ (45°, 60°, and 75°)] are fixed vertically at one end and pushed by the load cell at the other end horizontally at a constant speed, 10 mm min^{-1}.

A

Three-bulge molecule tubes x 4

Four-bulge molecule tubes x 3

B

Two-bulge molecule tubes x 5

Five-bulge molecule tubes x 2
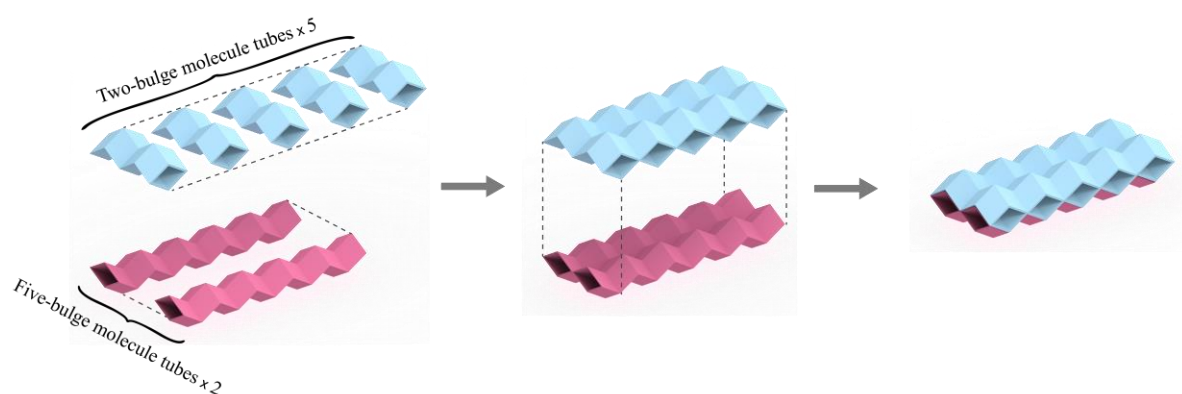
Figure S1. The structures of the OASS actuators created in this work. (A) The structure of the 3×4 OASS actuator for compression stiffness analysis. (B) The structure of the 2×5 OASS actuator for bending stiffness analysis.
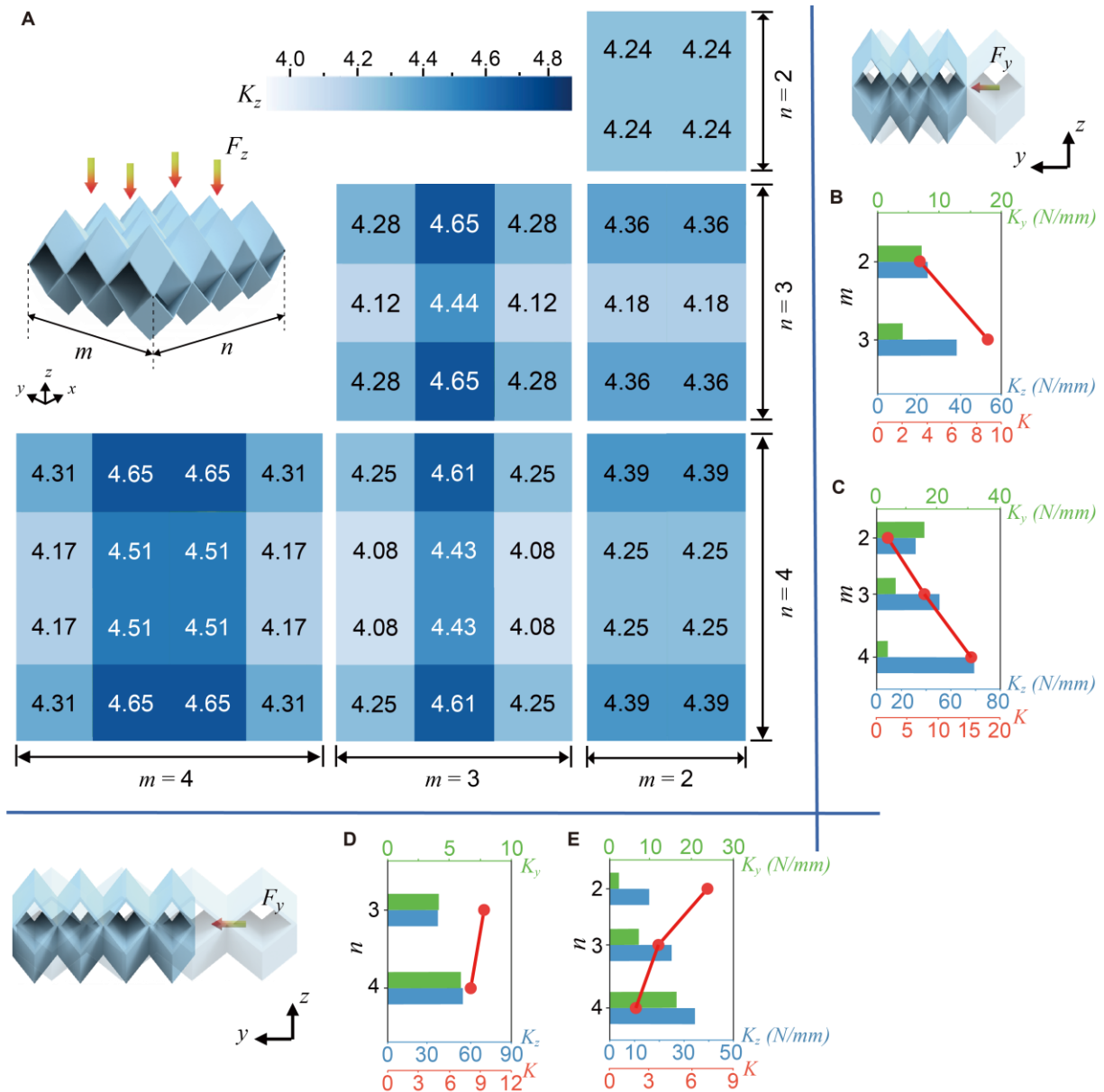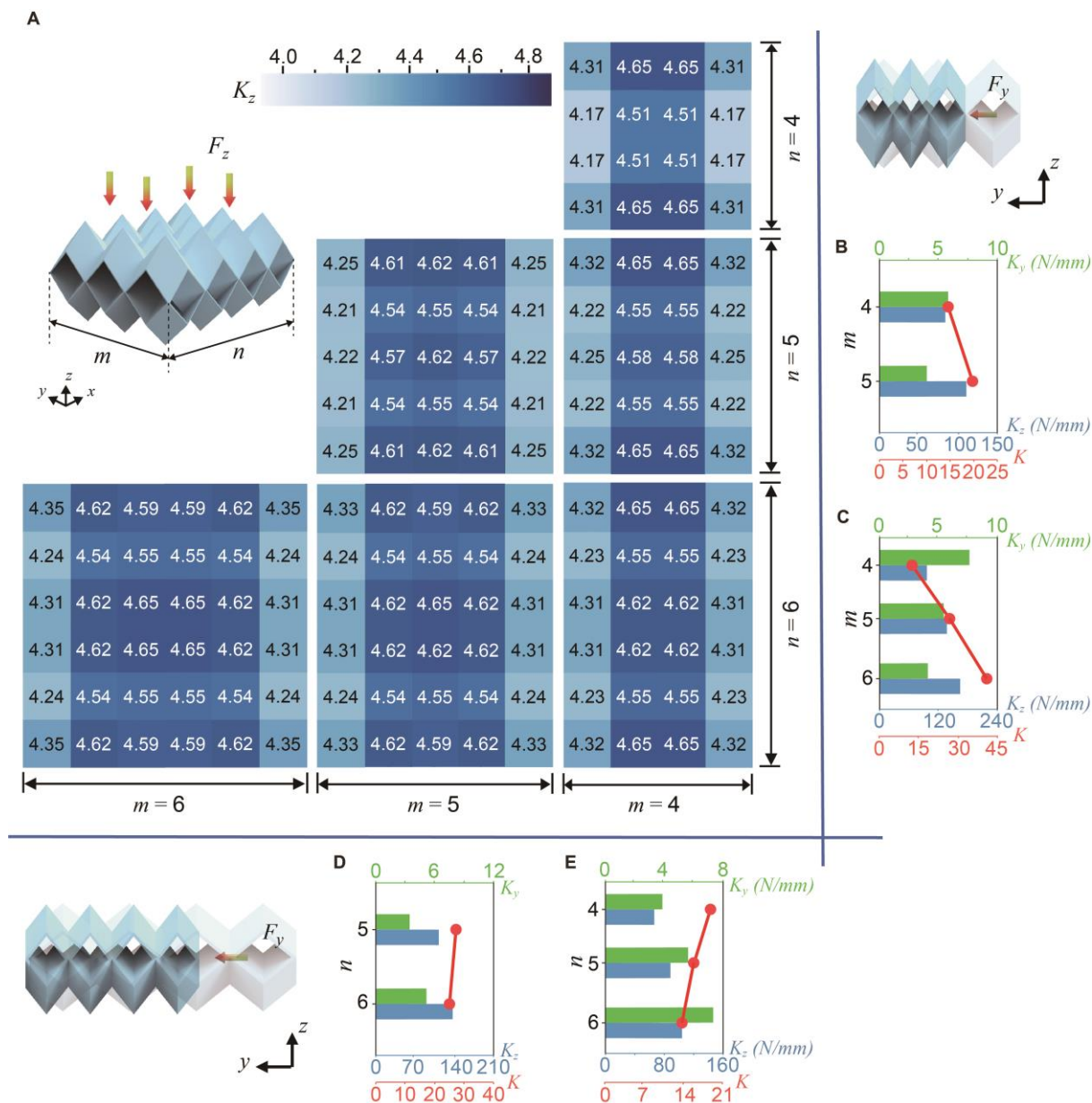
Figure S2. The anisotropic compression stiffness of OASS actuators under various values of $m \times n$ (m, n = 2, 3, and 4). (A) The compression stiffness K_z at each bulge for different m and n. The stiffness K_y, K_z, and K are represented by green, blue, and red, respectively, when (B) n = 3, (C) n = 4, (D) m = 3, and (E) m = 4.

6

Figure S3. The anisotropic compression stiffness of OASS actuators under various values of $m \times n$ (m, n = 4, 5, and 6). (A) The compression stiffness K_z at each bulge for different m and n. The stiffness K_y, K_z, and K are represented by green, blue, and red, respectively, when (B) $n = 5$, (C) $n = 6$, (D) $m = 5$, and (E) $m = 4$.
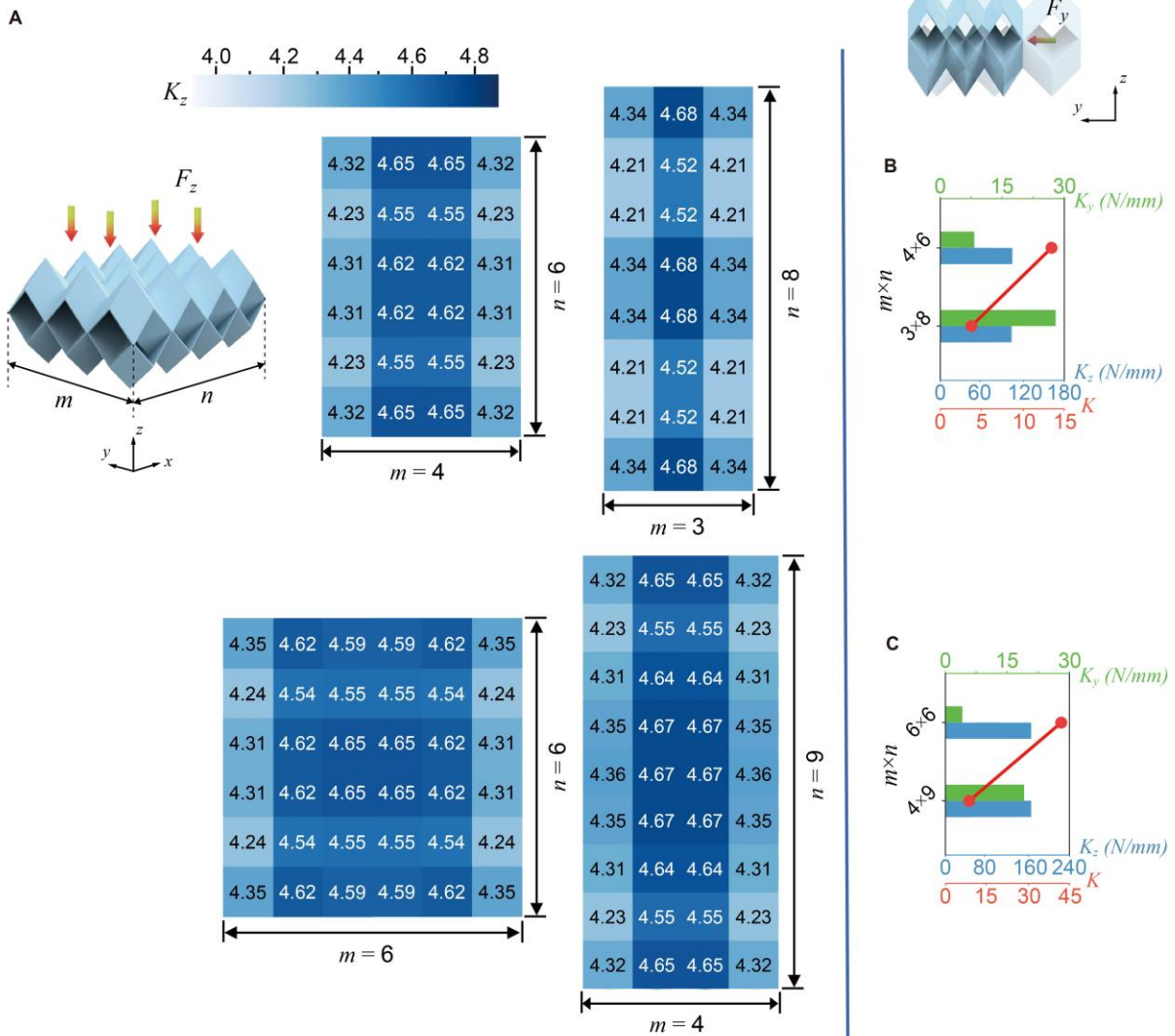
Figure S4. The anisotropic compression stiffness of OASS actuators under various values of $m \times n$ (4×6, 3×8, 6×6, and 4×9). (A) The compression stiffness K_z at each bulge for different m and n. The stiffness K_y, K_z, and K are represented by green, blue, and red, respectively when (B) $m \times n = 4 \times 6$ and 3×8, and (C) $m \times n = 6 \times 6$ and 4×9.
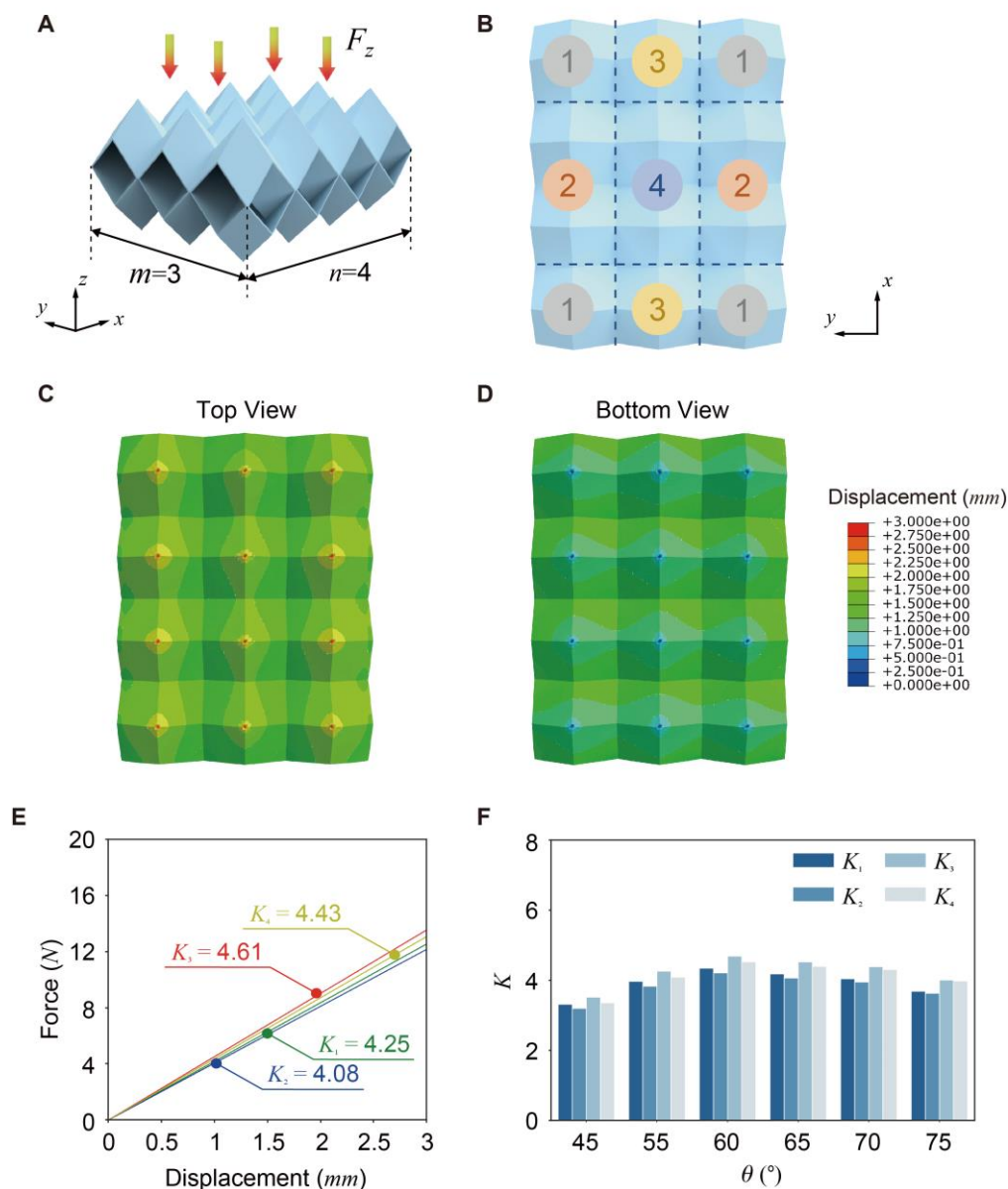
Figure S5. The anisotropic compression stiffness of the 3×4 OASS actuator in the *z*-direction. (A) Geometry of a 3×4 OASS actuator when F_z is applied in the *z*-direction. (B) The actuator is divided into four categories in the *x-y* plane depending on the edge conditions. (C, D) The top and bottom view of the displacement field in the OASS actuator under 3 mm displacements, respectively. Displacements are indicated in units of mm. (E) Compression stiffness K_z in four categories are represented by green, blue, red, and yellow, respectively. (F) Compression stiffness K_z in four categories under various values of θ are represented by four gradient colors from deep to light, respectively.
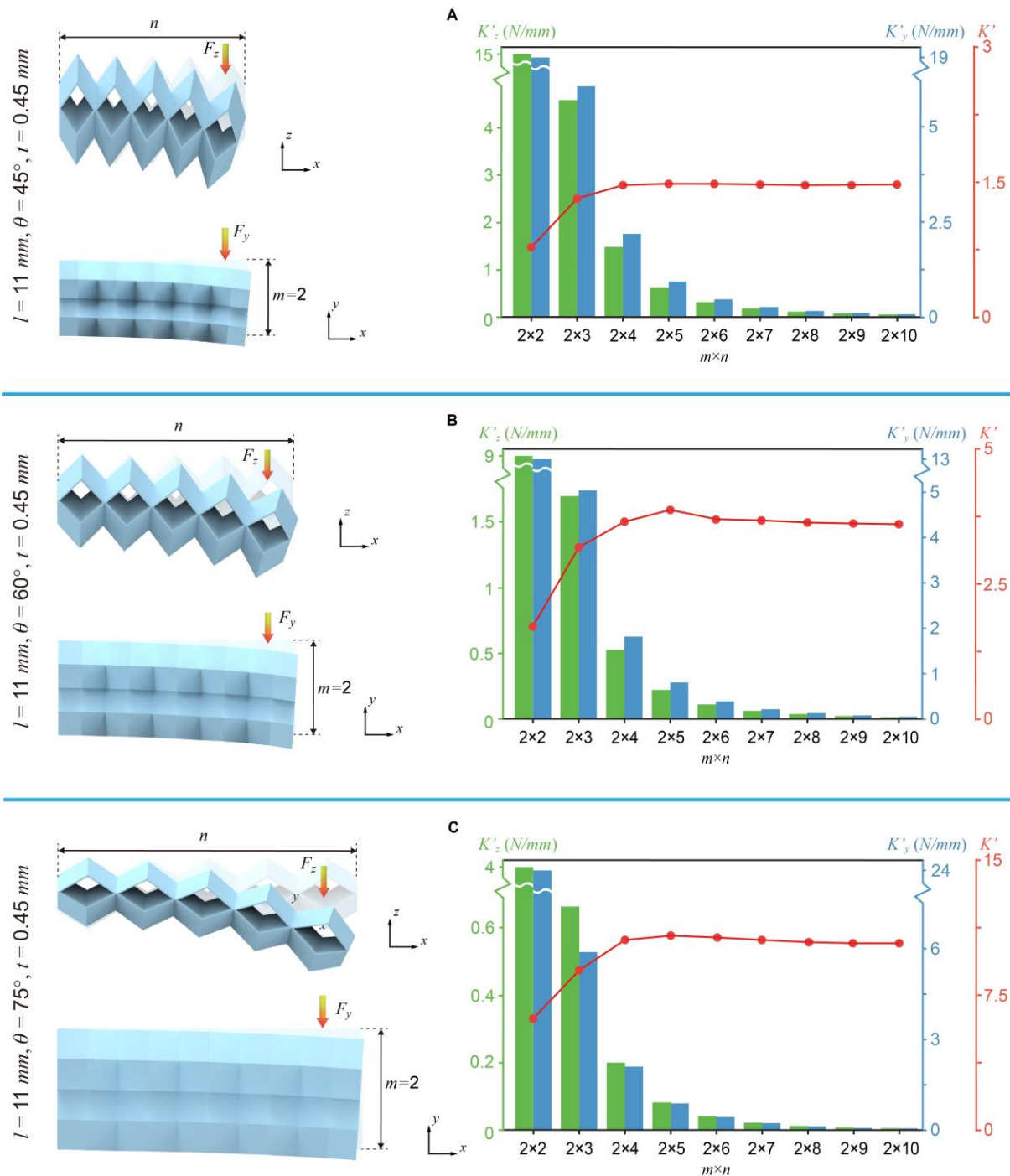
Figure S6. The anisotropic bending stiffness of OASS actuators under various values of *m×n* (*m*=2, *n*=2 to 10). K'_y, K'_z, and K' are represented by blue, green, and red, respectively, when (A) *θ* is 45°, (B) *θ* is 60°, and (C) *θ* is 75°.
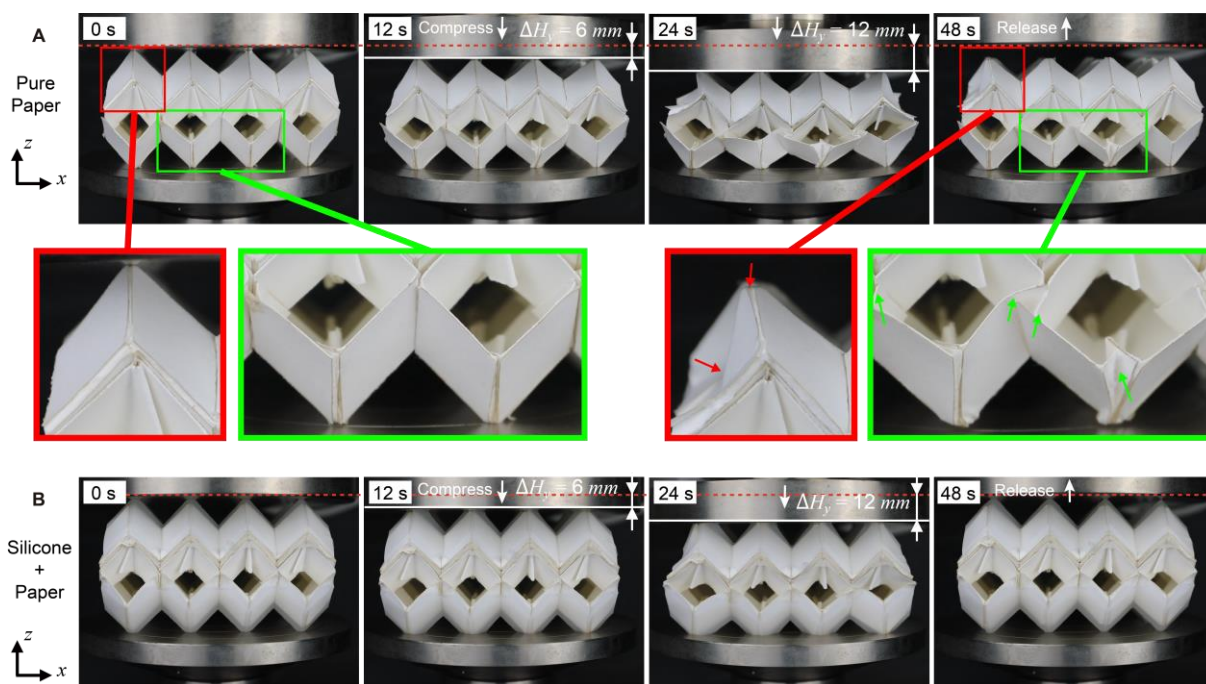
Figure S7. Compression tests on OASS actuators in the *z*-direction. The actuators are made by (A) PP and (B) SP, respectively.
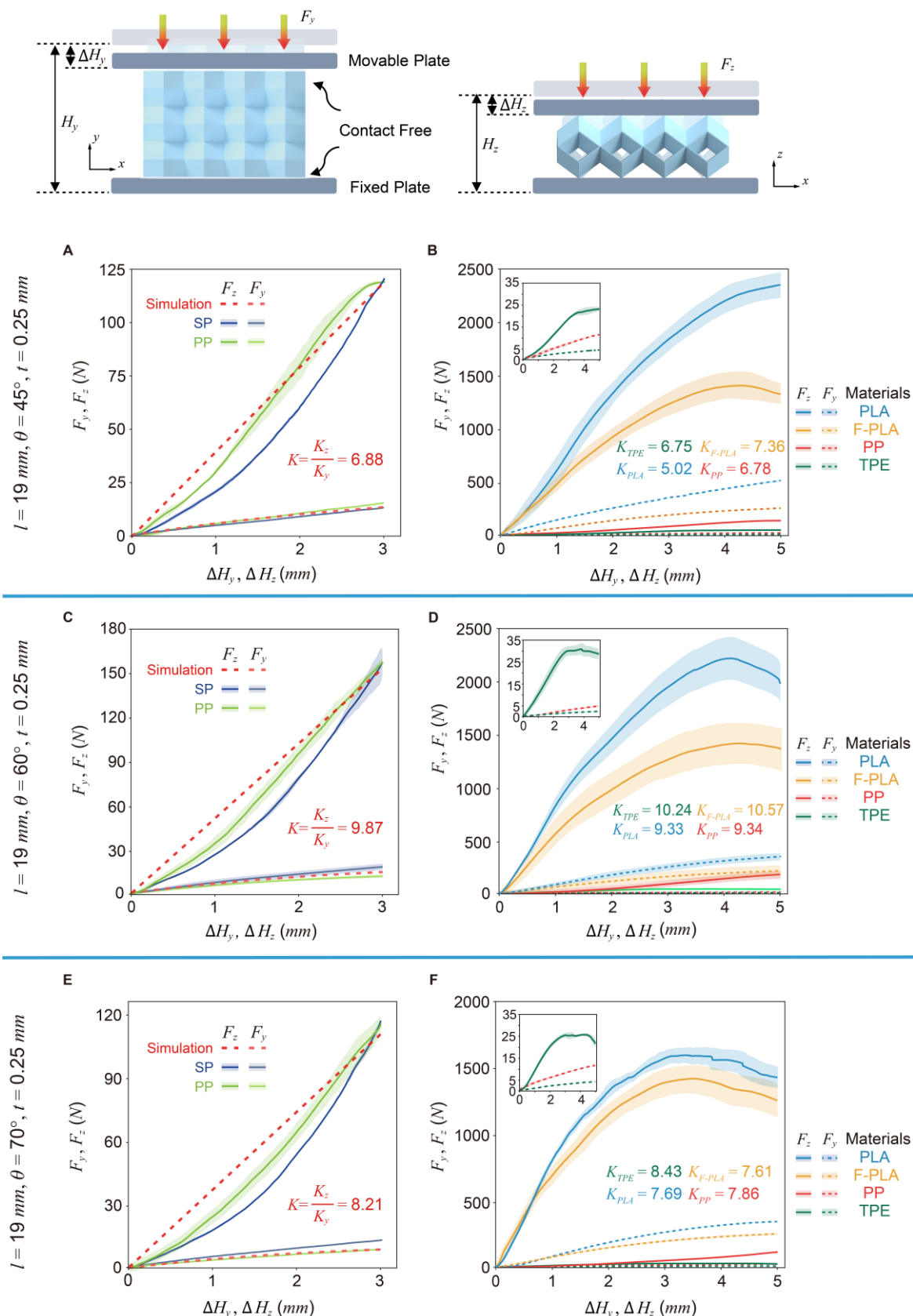
Figure S8. The anisotropic compression stiffness of OASS actuators made by different materials. The force-displacement curvatures of 3×4 OASS actuators made by different materials, when (A, B) θ is 45°, (C, D) θ is 60°, and (E, F) θ is 70°.
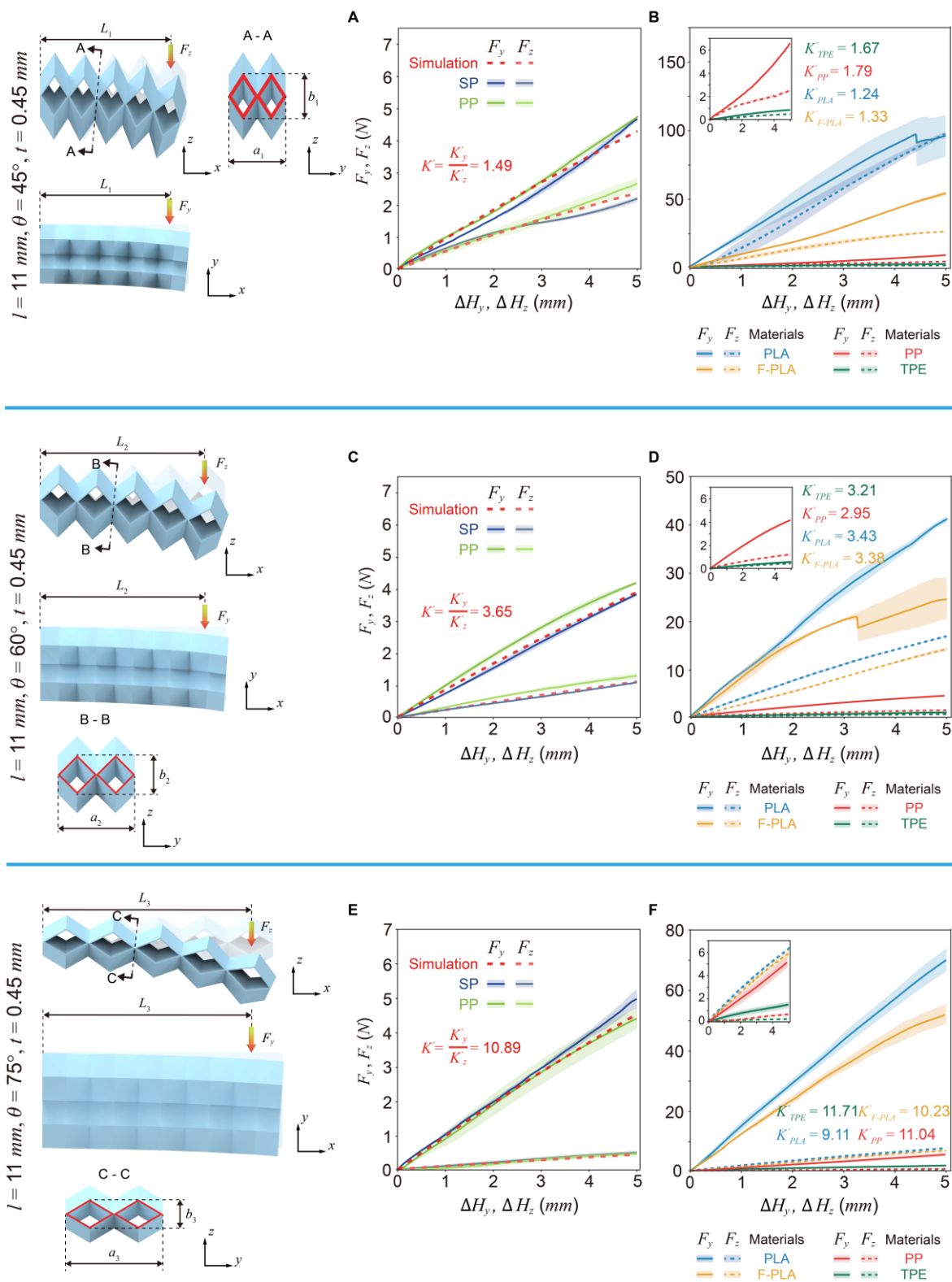
Figure S9. The anisotropic bending stiffness of OASS actuators made by different materials. The force-displacement curvatures of 2×5 OASS actuators made by different materials, when (A, B) θ is 45°, (C, D) θ is 60°, and (E, F) θ is 75°.
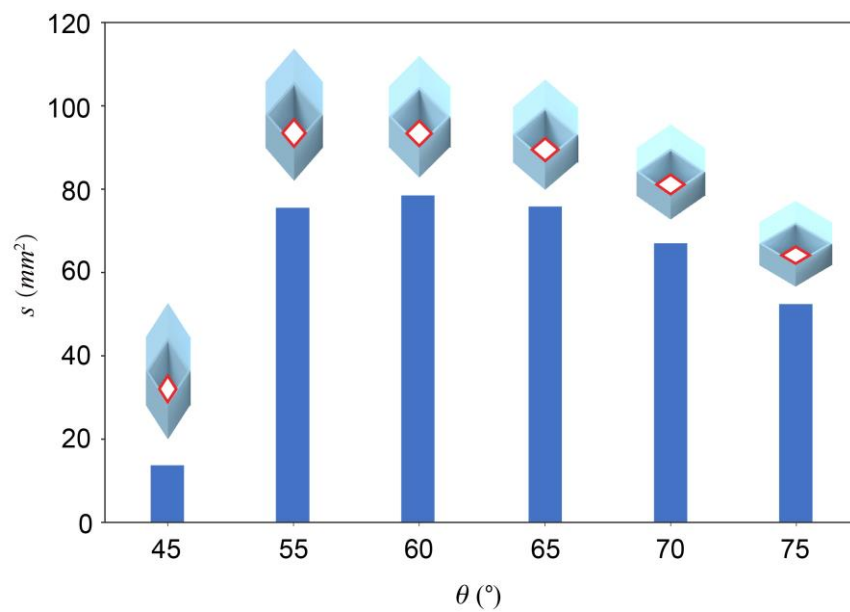
Figure S10. The cross-section area *s* of the airpath in OASS molecule tubes under various values of θ.
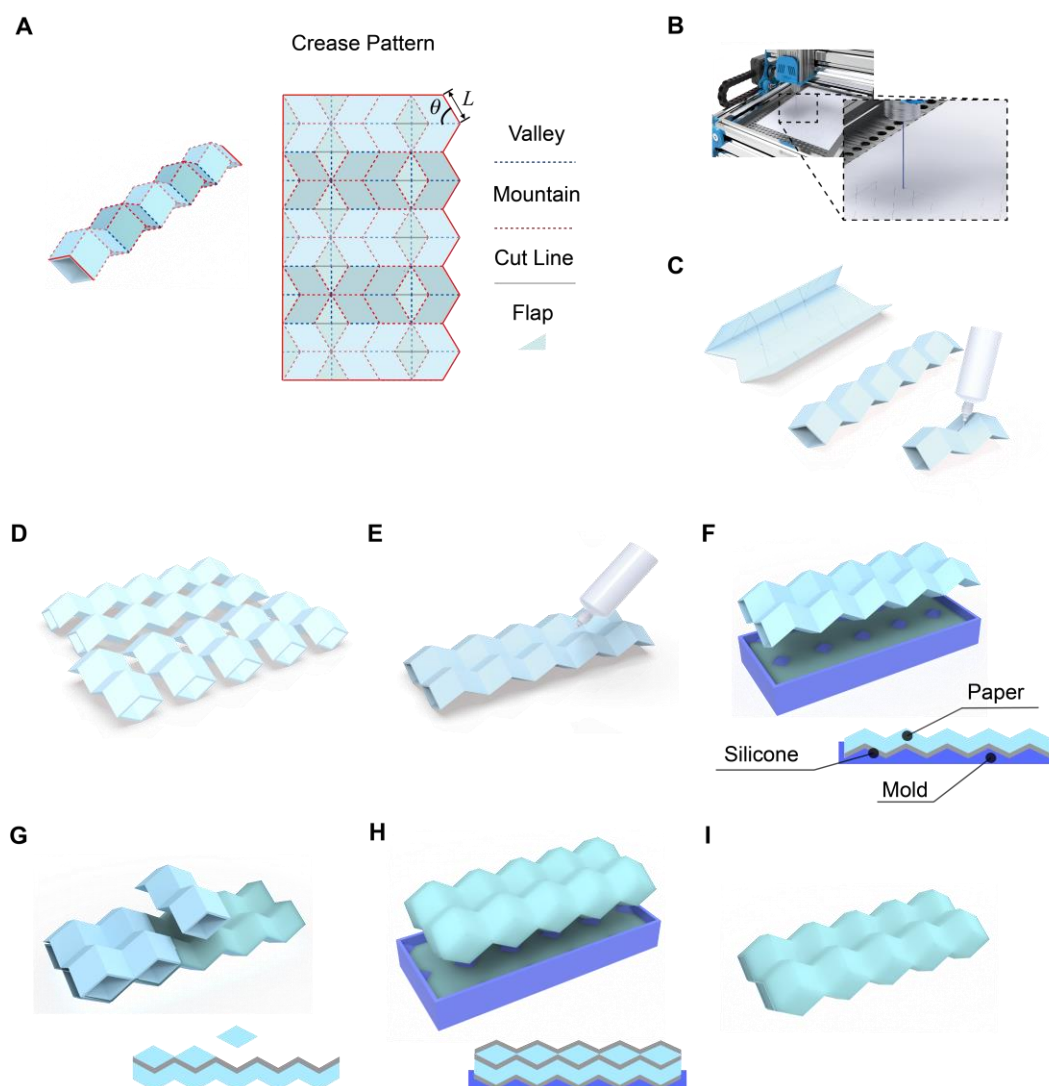
Figure S11. The fabrication process of an OASS actuator. (A) Folding scheme for a five-bulge molecule. (B) The paper is engraved using a CO_2 laser machine. (C) We fold the paper into bulges along the creases and glue openings. (D) The molecule tubes with different number of bulges are available for actuator fabrication. (E) Two five-bulge molecule tubes are assembled in parallel using instant cyanoacrylate gel. (F) Silicone layer is covered on the bulges using a mold. (G) Five two-bulge tubes are assembled upon the assembly of two five-bulge tubes. (H) The openings and the paper surfaces are covered by silicone rubber. (I) A typical prototype of OASS actuator is ready for robots.
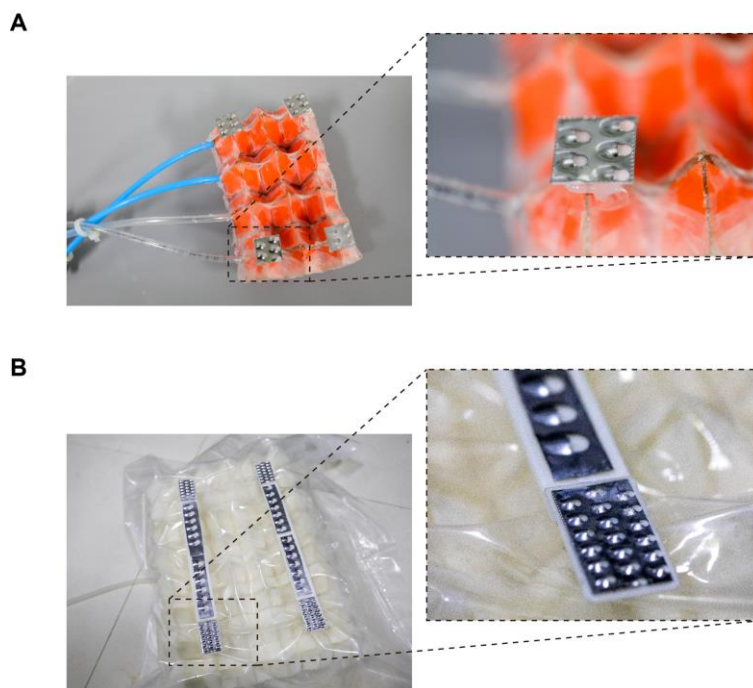
Figure S12. The directional friction feet at the bottom of crawling robots. (A) The directional friction feet on the small crawling robot. (B) The directional friction feet on the big crawling robot.
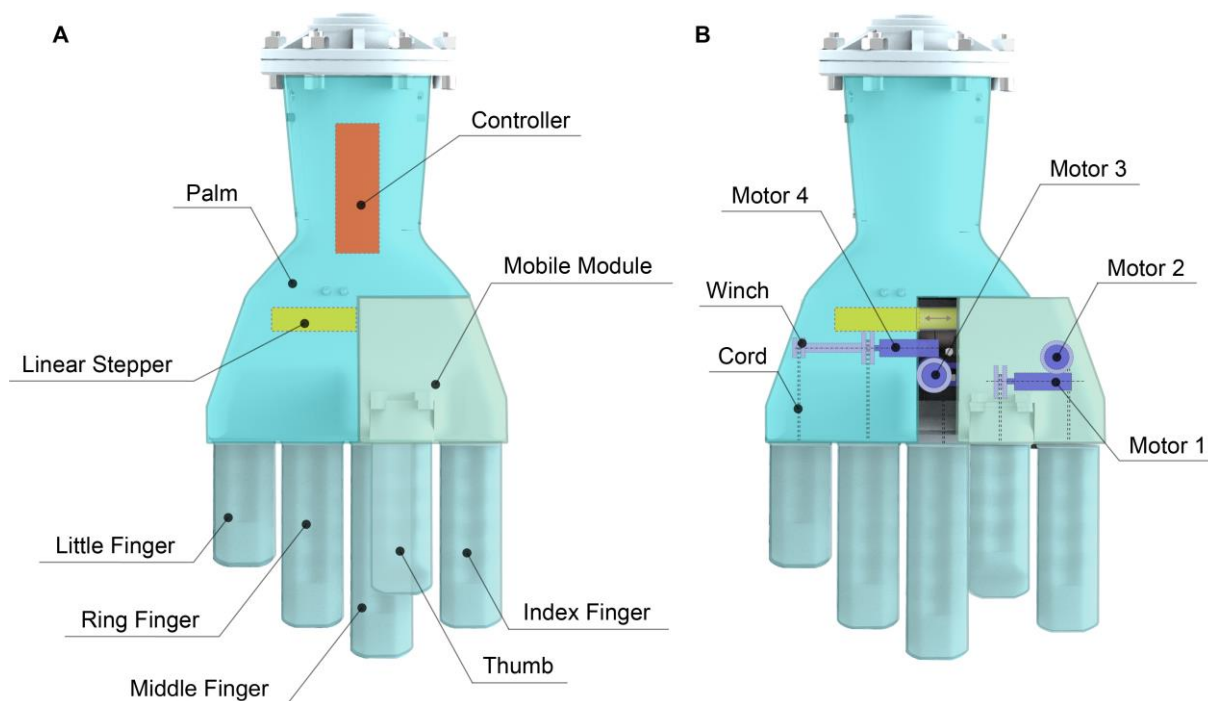

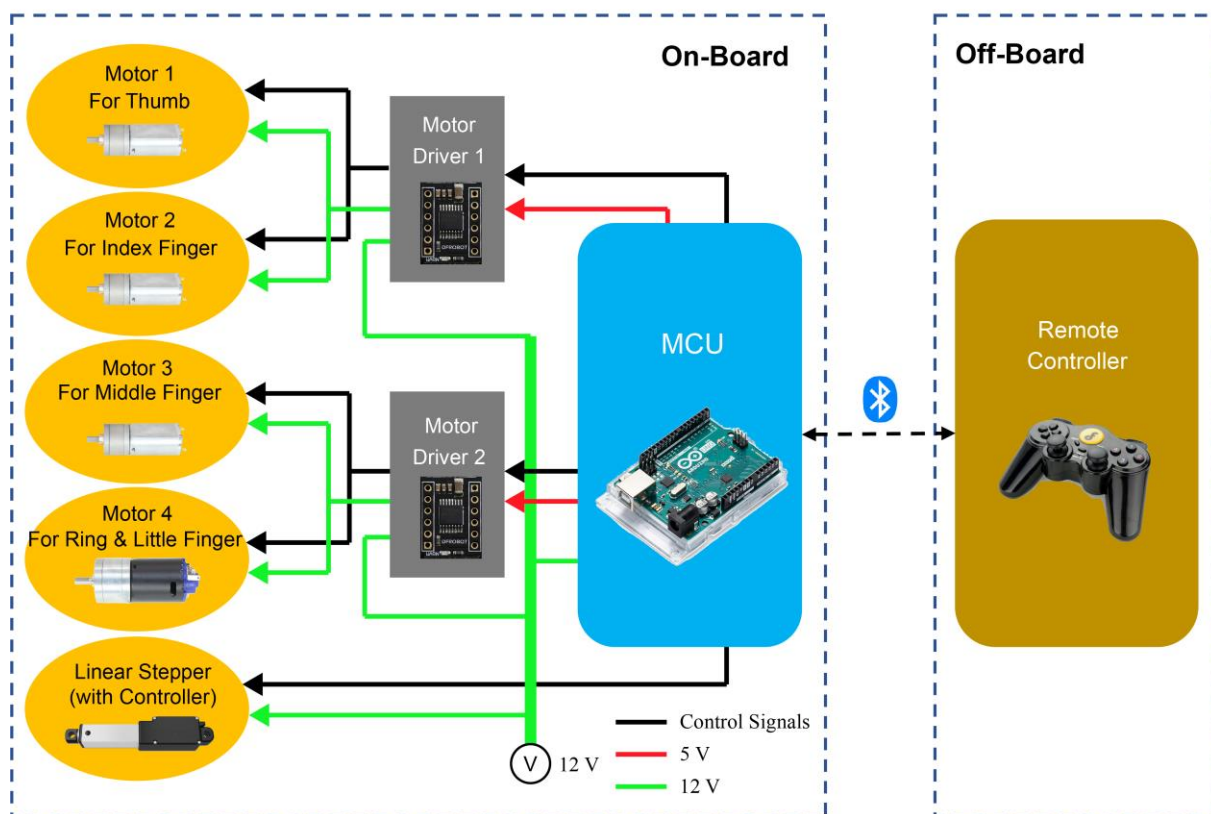**Figure S13.** Structure diagram of the OASS prosthetic hand.

System Topology

Figure S14. Control system topology diagram of the OASS prosthetic hand.

Table S1. Cost of OASS Prosthetic Hand

Component	Count	Unit cost	Extended cost
Body materials			
A4 paper (400 g/m^2)	6 sheets	$3.3/50 sheets	$0.4
Ecoflex 00-30	600 ml	$350/gallon	$56
eSUN PLA+	0.8 kg	$15.8/kg	$13
Power and control components			
Controller board	1	$17	$17
Remote controller	1	$36	$36
Motor driver	2	$5	$10
GM20-180 motor	3	$6	$18
GM25-370 motor	1	$5	$5
Linear stepper	1	$70	$70
Power supply	1	$38	$38
Total			$263.4

Movie S1. A small OASS-based crawling robot for heavy payload carrying.

Movie S2. A big OASS-based crawling robot for heavy payload carrying.

Movie S3. The OASS hand for irregular-shaped or fragile items grasping.

Movie S4. Comparison of the solid-soft hand and the OASS hand for plate items grabbing.

Movie S5. Comparison of the solid-soft hand and the OASS hand for large or heavy items lifting.

Movie S6. Comparison of the solid-soft hand and the OASS hand for bulky items on the plane fiddling.

Movie S7. Comparison of the solid-soft hand and the OASS hand bulky items at the corner of a box fiddling.

Movie S8. Comparison of the solid-soft hand and the OASS hand for an egg smashing.

Movie S9. Comparison of the solid-soft hand and the OASS hand for an item holding and vibrating.

Movie S10. The snake-shaped robot.

Movie S11. The snake-shaped robot moving out of buried by heavy objects.

Movie S12. The snake-shaped robot spanning in the air.

Movie S13. The process of folding the paper into an OASS molecule tube.